JOURNAL OF GUIDANCE, CONTROL, AND DYNAMICS
Vol. 30, No. 2, March–April 2007

Boundedness of Spacecraft Hovering Under Dead-Band Control in Time-Invariant Systems

Stephen B. Broschart* and Daniel J. Scheeres†
University of Michigan, Ann Arbor, Michigan 48109

DOI: 10.2514/1.20179

In this paper, we derive sufficient conditions for local and global boundedness of spacecraft motion inside a prescribed region subject to a dead-band hovering thrust control law in time-invariant Lagrangian dynamical systems. Using the conservative properties of the system, we define a zero-velocity restriction on the spacecraft motion, then show that a dead-band controller exists that bounds nearby trajectories arbitrarily close to the desired hovering position. The minimum number of independent directions that the dead band must restrict is well defined as a function of hovering position and divides the position space into distinct dynamical regions. We present numerical plots of these regions in the two-body, restricted three-body, and Hill problems and find hovering near a central body usually requires dead-band control in only one or two independent directions to be bounded. The effects of uncertainty in the initial hovering state on the zero-velocity surface are evaluated and the largest allowable perturbations in the Jacobi constant that maintain boundedness are formulated.

Nomenclature

$\boldsymbol{A}$	=	set of allowable spacecraft positions (localized formulation)
$\boldsymbol{B}$	=	set of allowable spacecraft positions (global formulation)
C_L	=	value of Jacobi constant in the Lagrangian formulation
C_0	=	nominal value of Jacobi constant
C^*	=	value of perturbed Jacobi constant
$\hat{\boldsymbol{c}}$	=	unit vector in dead-band thrust direction
$\boldsymbol{D}$	=	set of positions on the dead-band surface
d	=	function that defines the dead-band surface
f_{db}	=	dead-band function
G	=	function that defines the zero-velocity surface
J	=	Jacobi constant
J_{bf}	=	Jacobi constant for the two-body problem
J_{Hill}	=	Jacobi constant in the Hill three-body problem
J_{R3BP}	=	Jacobi constant in the restricted three-body problem
L	=	Lagrangian function
N	=	mean motion of the primaries' orbit
$\boldsymbol{p}$	=	generalized momenta of the system
$\boldsymbol{q}$	=	system configuration variables
$(\boldsymbol{q}_{\text{eqm}}, \dot{\boldsymbol{q}}_{\text{eqm}})$	=	equilibrium state in Lagrangian formulation
R	=	distance between primaries
R_c	=	dead-band surface radius
R_r	=	resonance radius
$r_{\max}$	=	maximum attainable distance from nominal
$\boldsymbol{r}_{\text{sc},1}, \boldsymbol{r}_{\text{sc},2}$	=	spacecraft position with respect to first/second primary
$\boldsymbol{r} = [x, y, z]^T$	=	spacecraft position vector
$\ddot{\boldsymbol{r}} = [\ddot{x}, \ddot{y}, \ddot{z}]^T$	=	spacecraft acceleration vector
$\boldsymbol{r}_0 = [x_0, y_0, z_0]^T$	=	nominal hovering position
$\boldsymbol{r}^* = [x^*, y^*, z^*]^T$	=	critical position where dead-band surface and zero-velocity surface are not transverse
T	=	kinetic energy
$\boldsymbol{T}$	=	spacecraft thrust vector
$\boldsymbol{T}_{\text{DB}}$	=	dead-band component of control thrust
T_m	=	constant magnitude of dead-band control thrust
$\boldsymbol{T}_{\text{OL}}$	=	open-loop component of control thrust
t	=	time
U	=	gravitational potential of the central body
V	=	potential function
$\hat{\boldsymbol{v}}_c$	=	unit vector defining dead-band orientation
$v_{\max}$	=	maximum attainable spacecraft velocity
$\boldsymbol{v}_+$	=	spacecraft velocity vector after dead-band thrust activation
$\boldsymbol{v}_-$	=	spacecraft velocity vector before dead-band thrust activation
$\boldsymbol{v} = [\dot{x}, \dot{y}, \dot{z}]^T$	=	spacecraft velocity vector
$\boldsymbol{Z}$	=	set of positions on the zero-velocity surface
β_{SRP}	=	force parameter for solar radiation pressure
γ	=	dead-band size parameter
ΔJ	=	perturbation from nominal Jacobi constant
$\Delta J_{\max}$	=	largest perturbation from nominal Jacobi constant
$\Delta J_+, \Delta J_-$	=	maximum allowable increase/decrease in Jacobi constant to preserve boundedness
$\delta\boldsymbol{r}$	=	deviation in position from nominal
$\delta\boldsymbol{r}_0$	=	error in initial position vector
$\delta\boldsymbol{v}$	=	deviation in velocity from nominal
$\delta\boldsymbol{v}_0$	=	error in initial velocity vector
$\delta v_{0,\max}$	=	maximal error in initial velocity that preserves boundedness
$\delta(x)$	=	Dirac's delta function
μ	=	ratio of masses, $\mu_2/(\mu_1 + \mu_2) \leq \frac{1}{2}$
μ_{CB}	=	gravitational parameter of the central body
μ_{SB}	=	gravitational parameter of the small body
μ_{Sun}	=	gravitational parameter of the sun
μ_1, μ_2	=	gravitational parameter of the first/second primary
$\tilde{\boldsymbol{\omega}} = [0, 0, \omega]^T$	=	frame angular velocity vector

Presented as Paper 381 at the 2005 AAS/AIAA Astrodynamics Specialists Conference, Lake Tahoe, CA, 8–11 August 2005; received 23 September 2005; revision received 14 March 2006; accepted for publication 29 April 2006.

*Ph.D. Candidate, Department of Aerospace Engineering, 2016 FXB. Student Member AIAA.

†Associate Professor, Department of Aerospace Engineering, 3048 FXB. Associate Fellow AIAA.

I. Introduction

IN recent years, there has been significant interest in sending spacecraft to small bodies in our solar system (including

asteroids, comets, and planetary satellites) for the purpose of scientific study. However, the dynamics of a spacecraft near such a body are greatly complicated by the irregular mass distribution of these bodies, their weak gravitational fields, and the nontrivial perturbations due to solar tide and radiation pressures. One strategy that has been proposed to mitigate these difficulties is hovering [1–3]. Hovering can be defined broadly as using control thrust to null the total acceleration on the spacecraft, creating an equilibrium at a desired position. This approach is feasible near small bodies because the nominal accelerations on a spacecraft are small.

Hovering near small bodies was first studied by Scheeres [1] in a paper that looked at the eigenvalue structure of hovering using an open-loop controller to cancel the spacecraft's nominal acceleration. Subsequent papers added a one-dimensional dead-band control on altitude to the open-loop thrust to suppress deviations from nominal and determined where motion could be stabilized by this controller analytically [2] and numerically [3]. The Japanese Aerospace Exploration Agency (JAXA) successfully implemented spacecraft hovering near an asteroid for the first time in the fall of 2005 during its Hayabusa mission to asteroid Itokawa. Kubota et al. [4] and Kominato et al. [5] document their three-dimensional dead-band hovering control approach and success in detail. In this paper, we use the conservative properties of spacecraft dynamics near small bodies to determine the minimal dimension dead-band controller that is sufficient to bound hovering motion at a given position. Our approach allows the region near the small body to be partitioned according to the type of dead band that bounds hovering. This result will help mission planners determine the minimal measurement capabilities necessary to maintain hovering at a chosen location.

The paper begins by defining the Jacobi constant for a class of dynamical systems applicable to spacecraft motion and formulating the zero-velocity surface near an equilibrium. We then show that a dead-band hovering controller does not destroy the conservative property of the system. The effects of uncertainty in initial state and thrust on the zero-velocity surface are presented, which leads to sufficient conditions for localized and global boundedness of hovering trajectories. The maximum allowable perturbation in initial state such that boundedness is preserved under dead-band control is defined. Finally, our sufficiency conditions are used to map the dead-band control necessary to bound hovering motion in the small-body-fixed frame, in the restricted three-body problem, and in the Hill three-body problem as a function of hovering position. The paper closes by discussing implementation of hovering using a reduced measurement set and a method of obtaining near-asymptotic stability.

II. Spacecraft Motion Near Equilibrium

The equations of motion for a spacecraft in a uniformly rotating coordinate frame subject to accelerations derived from a potential function and a constant thrust (in the rotating frame) can be written as

$$\ddot{\boldsymbol{r}} + 2(\tilde{\omega} \times \boldsymbol{v}) = \frac{\partial V(\boldsymbol{r}, t)}{\partial \boldsymbol{r}} + \boldsymbol{T} \tag{1}$$

where the angular velocity of the reference frame with respect to inertial space, $\tilde{\omega}$, is assumed to be constant. For the case of a single attracting body in the rotating frame, $V(\boldsymbol{r}, t) = U(\boldsymbol{r}, t) + 0.5\omega^2(x^2 + y^2)$, though more general forms are possible. If we multiply both sides of Eq. (1) by $\boldsymbol{v}$, we find

$$\frac{\mathrm{d}}{\mathrm{d}t}\left[\frac{1}{2}\boldsymbol{v}^T\boldsymbol{v} - V(\boldsymbol{r}, t) - \boldsymbol{T}^T\boldsymbol{r}\right] = -\frac{\partial V}{\partial t} \tag{2}$$

If we have chosen our reference frame such that V is not an explicit function of time (i.e., $\partial V/\partial t = 0$), then we have found the Jacobi constant for this system.

$$J(\boldsymbol{r}, \boldsymbol{v}) = \frac{1}{2}\boldsymbol{v}^T\boldsymbol{v} - V(\boldsymbol{r}) - \boldsymbol{T}^T\boldsymbol{r} \tag{3}$$

Table 1 Shapes of zero-velocity surfaces [6]

Sign of eigenvalues	Zero-velocity surface	$\|\boldsymbol{v}\| > 0$ surface
+,+,+	Imaginary quadratic cone	Imaginary ellipsoid
+,+,−	Real quadratic cone	Two-sheet hyperboloid
+,−,−	Real quadratic cone	One-sheet hyperboloid
−,−,−	Imaginary quadratic cone	Real ellipsoid

Equation (3) maintains its value for the duration of any trajectory following the equations of motion [Eq. (1)].

It is clear that we can always choose $\boldsymbol{T} = -[\partial V(\boldsymbol{r})/\partial \boldsymbol{r}]|_{(\boldsymbol{r}_0, \boldsymbol{0})}$ such that the right hand side of Eq. (1) equals zero at $\boldsymbol{r}_0$. If $\boldsymbol{v}$ is also zero, then we have an equilibrium point at $\boldsymbol{r}_0$. This is precisely the approach that is used in spacecraft hovering.

If we initialize a trajectory at an equilibrium state $(\boldsymbol{r}, \boldsymbol{v}) = (\boldsymbol{r}_0, \boldsymbol{0})$, then all states on a valid trajectory must satisfy the following equation.

$$J(\boldsymbol{r}, \boldsymbol{v}) = J(\boldsymbol{r}_0, \boldsymbol{0}) = C_0, \quad \forall\ t \tag{4}$$

If we expand the left-hand side in a Taylor series in position and velocity deviations from the equilibrium state to second order, we obtain the following condition on allowable states in the vicinity of the equilibrium,

$$\delta\boldsymbol{r}^T \left.\frac{\partial^2 J}{\partial \boldsymbol{r}^2}\right|_{(\boldsymbol{r}_0, \boldsymbol{0})} \delta\boldsymbol{r} = -\delta\boldsymbol{v}^T\delta\boldsymbol{v} \le 0 \tag{5}$$

where $\delta\boldsymbol{r} = \boldsymbol{r}(t) - \boldsymbol{r}_0$ and $\delta\boldsymbol{v} = \boldsymbol{v}(t)$. Note that $(\partial J/\partial \boldsymbol{r})|_{(\boldsymbol{r}_0, \boldsymbol{0})} = (\partial J/\partial \boldsymbol{v})|_{(\boldsymbol{r}_0, \boldsymbol{0})} = 0$ at an equilibrium point. It is clear that for real values of $\delta\boldsymbol{v}$, the right-hand side must be less than or equal to zero. This inequality defines the local region of allowable motion in position space of the system. The boundary of this region, where

$$\delta\boldsymbol{r}^T \left.\frac{\partial^2 J}{\partial \boldsymbol{r}^2}\right|_{(\boldsymbol{r}_0, \boldsymbol{0})} \delta\boldsymbol{r} = 0 \tag{6}$$

defines a quadratic "zero-velocity surface" as a function of $\delta\boldsymbol{r}$ that cannot be crossed by a real-valued system. This result for the zero-velocity surface near equilibria is general and applies to any time-invariant conservative system. A more general formulation is given in the appendix.

Depending on the signs of the eigenvalues of $(\partial^2 J/\partial \boldsymbol{r}^2)|_{(\boldsymbol{r}_0, \boldsymbol{0})}$, this boundary has one of the quadratic shapes described in Table 1. In simple terms, Table 1 means the following. If all three eigenvalues are negative, then there are no local restrictions on where the spacecraft can go as all displacements from nominal result in a negative left-hand side of Eq. (5). Conversely, if all eigenvalues are positive, then no displacements from the nominal state are permitted. For both of the mixed eigenvalue cases, the zero-velocity surface is a real quadratic cone in $\delta\boldsymbol{r}$ where the two bounding cones touch at the equilibrium point. For a real $\delta\boldsymbol{v}$, motion is restricted to hyperbolic surfaces on the outside of these cones in the +, −, − case and on the inside of the cones for the +, +, − case. The shaded region in Fig. 1 illustrates the allowable region of motion for each case in two dimensions. Each shaded contour represents allowable positions for some $\|\boldsymbol{v}\| \ge 0$.

III. Conservative Properties of Hovering Control

Now we show that the Jacobi constant defined in the preceding section holds for a spacecraft subject to an idealized dead-band hovering thrust controller. Previous work [3] defines dead-band hovering control as a sum of two thrust components: a constant, open-loop thrust to create an equilibrium at the desired hovering position, $\boldsymbol{T}_{\mathrm{OL}}$, and a dead-band thrust to control deviations from this nominal position, $\boldsymbol{T}_{\mathrm{DB}}$.

$$\boldsymbol{T}_{\mathrm{OL}} = -\left.\frac{\partial V}{\partial \boldsymbol{r}}\right|_{(\boldsymbol{r}_0, \boldsymbol{0})} \tag{7}$$

$$\boldsymbol{T}_{\mathrm{DB}} = \begin{cases} -T_m \hat{\boldsymbol{c}}(\boldsymbol{r}), & \text{if } f_{\mathrm{db}}(\boldsymbol{r}) \geq \gamma; \\ 0, & \text{otherwise} \end{cases} \tag{8}$$

If we assume that T_m is large so that the spacecraft does not move much outside the dead band [when $f_{\mathrm{db}}(\boldsymbol{r}) \geq \gamma$] before the thrust returns it, we can ignore the small external acceleration on the spacecraft derived from $V(\boldsymbol{r})$ during this time. Such a large thrust assumption is typically used and is reasonable for spacecraft applications. These assumptions allow a closed-form solution for the delta-V applied to the spacecraft between subsequent dead-band crossings as a function of incoming velocity. If we also require the dead-band thrust direction be normal to the dead-band boundary [$\hat{\boldsymbol{c}}(\boldsymbol{r}) = \nabla \hat{f}_{\mathrm{db}}(\boldsymbol{r})$], we obtain the impulsive form of the dead-band thrust component.

$$\boldsymbol{T}_{\mathrm{DB}} = -\{[2\boldsymbol{v}^T \nabla \hat{f}_{\mathrm{db}}(\boldsymbol{r})] \nabla \hat{f}_{\mathrm{db}}(\boldsymbol{r})\} \delta[f_{\mathrm{db}}(\boldsymbol{r}) - \gamma] \tag{9}$$

The dead-band function f_{db} would likely be based on altitude or position of the spacecraft and can be chosen to constrain the spacecraft motion in an arbitrary number of directions. The following examples of the function f_{db} would restrict spacecraft motion in one [Eq. (10)], two [Eq. (11)], or three [Eq. (12)] dimensions.

$$f_{\mathrm{db}}(\boldsymbol{r}) = |(\boldsymbol{r} - \boldsymbol{r}_0)^T \hat{\boldsymbol{v}}_c| \tag{10}$$

$$f_{\mathrm{db}}(\boldsymbol{r}) = \|(I - \hat{\boldsymbol{v}}_c \hat{\boldsymbol{v}}_c^T)(\boldsymbol{r} - \boldsymbol{r}_0)\| \tag{11}$$

$$f_{\mathrm{db}}(\boldsymbol{r}) = \|(\boldsymbol{r} - \boldsymbol{r}_0)\| \tag{12}$$

Level sets for each of these examples are shown in Fig. 2. There are many other possible formulations for f_{db}. The function should be chosen such that ∇f_{db} is well-defined at all relevant locations [i.e., smooth at the boundary $f_{\mathrm{db}}(\boldsymbol{r}) = \gamma$].

The formulation for the Jacobi constant [Eq. (3)] already allows for a constant thrust, so the conservative properties of this system are not violated for the $\boldsymbol{T}_{\mathrm{OL}}$ component of the hovering control. It is easily shown that the same Jacobi constant is preserved in the presence of the idealized dead-band thrust $\boldsymbol{T}_{\mathrm{DB}}$ as well. This impulsive thrust "reflects" the velocity vector of the spacecraft off the boundary $f_{\mathrm{db}}(\boldsymbol{r}) = \gamma$ such that

$$\boldsymbol{v}_+ = \boldsymbol{v}_- - 2(\boldsymbol{v}_-^T \hat{\boldsymbol{c}}) \hat{\boldsymbol{c}} \tag{13}$$

It is easily shown that the magnitude of the velocities before and after the burn are equal. Because the Jacobi constant depends only on the magnitude of $\boldsymbol{v}$, the addition of the impulsive control thrust $\boldsymbol{T}_{\mathrm{DB}}$ does not destroy the conservative nature of this class of dynamical systems.

IV. Hovering Control and Zero-Velocity Surfaces

Because dead-band hovering control does not destroy the Jacobi constant of our system, we can apply our knowledge of zero-velocity surfaces [Eq. (6) and Table 1] to design a controller that ensures boundedness of a hovering trajectory. The idea is to use dead-band thrust to control motion in the directions not naturally restricted by the zero-velocity surface. The general rule for hovering dead-band design is that the chosen controller must restrict motion in at least as many dimensions as the zero-velocity surface allows unrestricted motion and be oriented such that the spacecraft trajectory is trapped inside a bounded region defined by the zero-velocity surface and the dead-band surface.

For instance, say hovering is implemented at a position where the Hessian matrix of the Jacobi constant with respect to position has one negative and two positive eigenvalues (+, +, − case). Then if we orient a one-dimensional dead-band control of the form in Eq. (10) such that $\hat{\boldsymbol{v}}_c$ is sufficiently close to the eigenvector corresponding to the negative eigenvalue, the spacecraft trajectory is known to be bounded for all future time. Geometrically, the +, +, − zero-velocity surface defines a quadratic cone that restricts the spacecraft motion in two dimensions and the dead-band control defines two bounding planes that place "caps" on these cones. This creates a three-dimensional hourglass-shaped region of space to which the spacecraft is energetically restricted. Similarly in the +,−,− case, where the zero-velocity surface restricts motion in one dimension, a two-dimensional dead-band control, such as Eq. (11) with $\hat{\boldsymbol{v}}_c$ adequately close to the eigenvector corresponding to the positive eigenvalue, is sufficient to bound the nominal trajectory in three dimensions. In the −, −, − case, a dead-band control that bounds the trajectory in three dimensions, such as Eq. (12), would be necessary. Motion near equilibrium in the +, +, + case is stable without any control, but generally does not occur in astrodynamical systems.

Of course this idea works for the nominal system because there is no motion away from the equilibrium at all. The following sections show that this idea remains valid when uncertainties in the initial state and thrust are considered.

V. Local Boundedness

A. Perturbed Local Zero-Velocity Surfaces

First, we evaluate the effects of small errors in the initial state and control thrust on our localized zero-velocity surface result. The zero-velocity surface for hovering with small perturbations in initial position and velocity is defined via a Taylor expansion. In this way, the true value of the Jacobi constant can be approximated to second order as

$$J(\boldsymbol{r}_0 + \delta\boldsymbol{r}_0, \delta\boldsymbol{v}_0) = C^* \approx C_0 + \frac{1}{2}\delta\boldsymbol{r}_0^T \left.\frac{\partial^2 J}{\partial \boldsymbol{r}^2}\right|_{(\boldsymbol{r}_0, \boldsymbol{0})} \delta\boldsymbol{r}_0 + \frac{1}{2}\delta\boldsymbol{v}_0^T \delta\boldsymbol{v}_0 \tag{14}$$

For dynamically valid future motion,

$$J(\boldsymbol{r}_0 + \delta\boldsymbol{r}, \delta\boldsymbol{v}) = J(\boldsymbol{r}_0 + \delta\boldsymbol{r}_0, \delta\boldsymbol{v}_0) = C^* \tag{15}$$

and thus,

$$\delta\boldsymbol{r}^T \left.\frac{\partial^2 J}{\partial \boldsymbol{r}^2}\right|_{(\boldsymbol{r}_0, \boldsymbol{0})} \delta\boldsymbol{r} \approx -\delta\boldsymbol{v}^T \delta\boldsymbol{v} + 2(C^* - C_0) \tag{16}$$

We can define the zero-velocity surface for the system under small perturbations as

$$\delta\boldsymbol{r}^T \left.\frac{\partial^2 J}{\partial \boldsymbol{r}^2}\right|_{(\boldsymbol{r}_0, \boldsymbol{0})} \delta\boldsymbol{r} = 2(C^* - C_0) = \Delta J \tag{17}$$

In general, the quantity ΔJ can be positive or negative. The shape of the perturbed zero-velocity surface for all eigenvalue cases is given in Table 2. In all eigenvalue cases, the number of dimensions restricted by the zero-velocity surface and its orientation (eigenvectors) are not changed by small perturbations in initial state. This means that a dead-band control that bounds the nominal trajectory still has the dimensionality and the proper orientation to bound the perturbed trajectory (assuming small perturbations). For instance, in the +, +, − case, the zero-velocity surface is either a one-sheet or two-sheet hyperboloid. (In Fig. 1, the contours for $\|\boldsymbol{v}\| > 0$ in the +, +, − case are two-sheet hyperboloids and the contours in the +, −, − case are one-sheet hyperboloids.) Hovering in either of these cases would still be bounded by a one-dimensional dead-band control designed for the nominal state. This analytical result is verified by numerical simulation. Figure 3 shows an integrated hovering trajectory in the +, +, − region above a sphere and the predicted zero-velocity surface (dotted region). The trajectory

Table 2 Shape of zero-velocity surfaces for perturbed equilibria [6]

Sign of eigenvalues	$\Delta J > 0$	$\Delta J < 0$
+,+,+	Real ellipsoid	N/A
+,+,−	One-sheet hyperboloid	Two-sheet hyperboloid
+,−,−	Two-sheet hyperboloid	One-sheet hyperboloid
−,−,−	Imaginary ellipsoid	Real ellipsoid

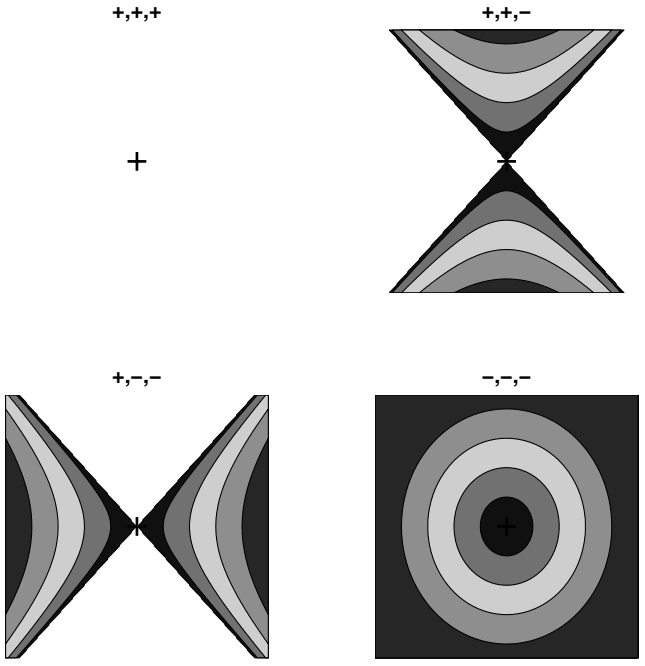

Fig. 1 Allowable regions of motion for different eigenvalue sets (shaded regions); each contour represents allowable positions for some nonnegative velocity magnitude.

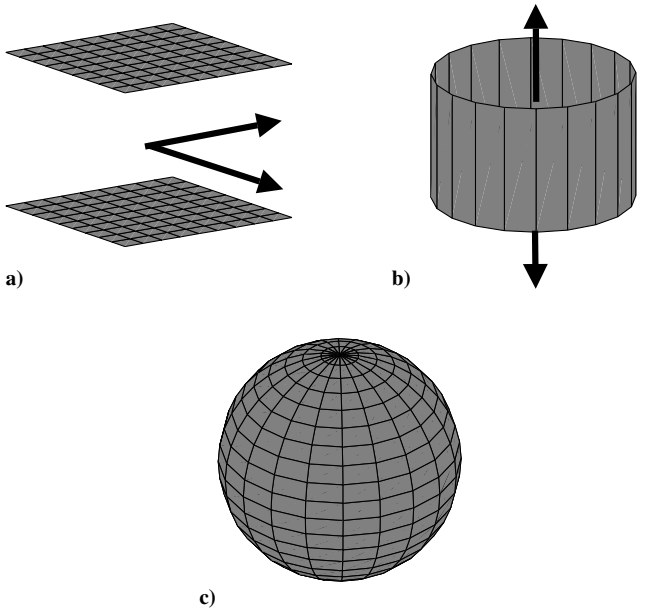

Fig. 2 Level sets of example dead-band functions: a) 1-D, b) 2-D, c) 3-D; arrows indicate direction of unrestricted motion.

remains contained in the predicted region for the full integration time ($\approx$1 day) under the nominally selected one-dimensional dead-band control.

Next, we can make a broader statement about the effect of uncertainty in the initial position without approximation. If we believe ourselves to be at position $\boldsymbol{r}$ when, in actuality, we are at $\boldsymbol{r} + \delta\boldsymbol{r}_0$, the equation for the local bounding zero-velocity surface is

$$(\delta\boldsymbol{r} - \delta\boldsymbol{r}_0)^T \left.\frac{\partial^2 J}{\partial \boldsymbol{r}^2}\right|_{(\boldsymbol{r}+\delta\boldsymbol{r}_0,\boldsymbol{0})} (\delta\boldsymbol{r} - \delta\boldsymbol{r}_0) + 2\left.\frac{\partial J}{\partial \boldsymbol{r}}\right|_{(\boldsymbol{r}+\delta\boldsymbol{r}_0,\boldsymbol{0})} (\delta\boldsymbol{r} - \delta\boldsymbol{r}_0) = 0 \tag{18}$$

where $(\partial J/\partial \boldsymbol{r})|_{(\boldsymbol{r}+\delta\boldsymbol{r}_0,\boldsymbol{0})} \neq 0$ because $\boldsymbol{T}_{\mathrm{OL}}(\boldsymbol{r})$ does not create an equilibrium point. In general, this quadratic is not centered at $\boldsymbol{r} + \delta\boldsymbol{r}_0$. The center and ΔJ, which is not zero in general, can be found by completing the square. The shape of the zero-velocity surface still depends solely on the eigenvalues of the matrix $(\partial^2 J/\partial \boldsymbol{r}^2)|_{(\boldsymbol{r}+\delta\boldsymbol{r}_0,\boldsymbol{0})}$, and can be found in Table 2. This tells us that for the perturbed system to be bounded under dead-band hovering control, the actual initial position of the spacecraft must have the same eigenvalue signs as the nominal position. In addition, the eigenvectors that describe the true zero-velocity surface (linearized about $\boldsymbol{r} + \delta\boldsymbol{r}_0$) must be sufficiently close to the nominal so that the nominal dead band still bounds the motion in three dimensions. Thus, we can conclude that hovering near a "border" between different eigenvalue regions with a minimal dead-band control would risk unbounded behavior.

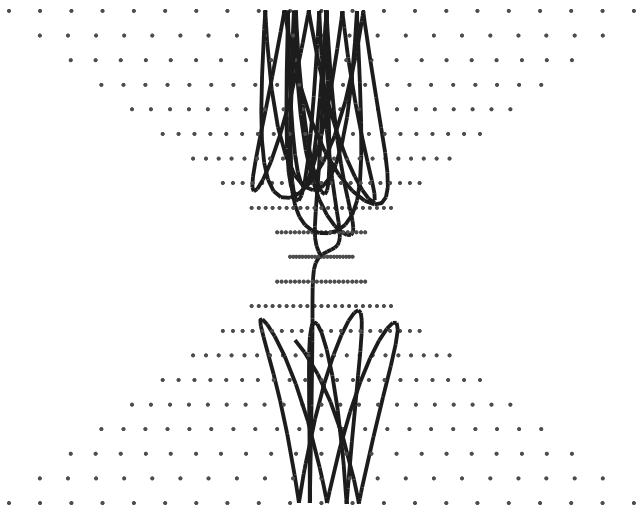

Fig. 3 Example of a +,+,− simulated trajectory; dots indicate the predicted region of allowable motion.

The effect of open-loop thrust application errors on the zero-velocity surface can be analyzed similarly. Both thrust and position errors cause $(\partial J/\partial \boldsymbol{r})|_{(\boldsymbol{r}_0,\boldsymbol{0})}$ to be nonzero, which changes the center of the bounding surface as well as its shape. However, the signs of the eigenvalues of $(\partial^2 J/\partial \boldsymbol{r}^2)|_{(\boldsymbol{r}_0,\boldsymbol{0})}$ and the orientation of the zero-velocity surface do not change from nominal, so the nominal controller will still bound the perturbed system.

B. Boundary Definition

Formally, we can show (uniform) boundedness of the trajectory using the definition of Khalil [7]. It states that the solutions of our dynamical system under a chosen hovering thrust control law are uniformly bounded if there exists a positive constant c, independent of $t_0 \geq 0$, and for every $a \in (0, c)$, there is $\beta = \beta(a) > 0$, independent of t_0, such that

$$\|x(t_0)\| \leq a \Rightarrow \|x(t)\| \leq \beta, \quad \forall\ t \geq t_0 \tag{19}$$

Because this system is time-invariant, the conditions regarding uniformity are automatically satisfied. For the proof, we use the standard norm and let $c = \gamma$, the parameter of the chosen dead band. In the initial condition ball of measure a, we first compute the largest ΔJ induced by any initial state

$$\Delta J_{\max} = \max_{(\boldsymbol{r},\boldsymbol{v})\in B_a} [J(\boldsymbol{r}, \boldsymbol{v}) - C_0] \tag{20}$$

and use it to compute the maximum allowable deviation in position and velocity from the nominal. Formally, if

$$\boldsymbol{A} = \left\{ \boldsymbol{r} \in \Re^3 \left| \delta\boldsymbol{r}^T \left.\frac{\partial^2 J}{\partial \boldsymbol{r}^2}\right|_{(\boldsymbol{r}_0,\boldsymbol{0})} \delta\boldsymbol{r} \leq \Delta J_{\max} \quad \text{and} \quad f_{\mathrm{db}}(\boldsymbol{r}) \leq \gamma \right. \right\} \tag{21}$$

then

$$r_{\max} = \max_{\boldsymbol{r}\in \mathrm{Bd}(\boldsymbol{A})} \|\boldsymbol{r} - \boldsymbol{r}_0\| \tag{22}$$

and

$$v_{\max} = \sqrt{2\{J_0 + \Delta J_{\max} + \max_{\boldsymbol{r}\in \boldsymbol{A}}[V(\boldsymbol{r}) + \boldsymbol{T}_{\mathrm{OL}}^T \boldsymbol{r}]\}} \tag{23}$$

If both $r_{\max}$ and $v_{\max}$ are finite, which is implied by our condition that the dead band must be properly oriented, then the system is bounded with $\beta(a) = r_{\max} + v_{\max}$.

Thus, a sufficient condition for boundedness of trajectories in the vicinity of the hovering position is that the chosen controller must restrict motion in at least as many dimensions as the zero-velocity surface allows unrestricted motion and be oriented such that the spacecraft trajectory is trapped inside a bounded region defined by the zero-velocity surface and the dead-band surface. To get this result, we have assumed that T_m is sufficiently large so that our impulsive approximation is valid (which makes the level set $f_{\mathrm{db}} = \gamma$ an inviolable boundary) and that γ is sufficiently small so that our second-order approximation of the zero-velocity surface is valid. Also, nothing here (except performance of the thruster) prevents using a very small γ to force $\boldsymbol{A}$ to be arbitrarily small.

This sufficient condition for boundedness is stronger than the sufficiency conditions for linear stability on the manifold for one-dimensional dead-band control presented in the previous literature [2] because it does not neglect the Coriolis forces on the spacecraft [3] nor artificially restrict the spacecraft motion. This boundedness test is also preferable to numerical studies [3] as it ensures bounded motion for all time and does not require numerical integration. Our result is a sufficient condition, however, and does not disagree with the stable (bounded) hovering regions predicted under open-loop control in previous literature [1].

For particular cases, computing $r_{\max}$ and $v_{\max}$ is simple algebra. For example, if we use the one-dimensional dead-band function in Eq. (10) with $\hat{\boldsymbol{v}}_c = \boldsymbol{v}_3$ at a hovering position with $+, +, -$ eigenvalue structure, then

$$r_{\max} = \sqrt{\gamma^2\left(1 - \frac{e_3}{e_1}\right) + \frac{\Delta J_{\max}}{e_1}} \tag{24}$$

and

$$v_{\max} = \sqrt{2(\Delta J_{\max} + \gamma^2 e_3^2)} \tag{25}$$

where e_3 is the negative eigenvalue, $\boldsymbol{v}_3$ is its corresponding eigenvector, and e_1 is the smaller of the positive eigenvalues.

This system is somewhat misleading due to its second-order nature as it allows for arbitrarily large increases in the nominal Jacobi constant without destroying boundedness. This is not the case in general as is shown in the next section.

VI. Global Boundedness

A. Boundary Definition

Now we show boundedness of hovering trajectories with perturbations in the initial state in a global formulation. This result would be more applicable than the localized result when using a dead band with a large γ. The argument is intuitive and simply states that for a trajectory to be bounded, its region of allowable motion must be finite.

In the formal boundedness definition (Sec. V.B), let $c = \gamma$ and $\Delta J_{\max}$ be defined as in Eq. (20). The allowable region of motion is defined as the set

$$\begin{aligned}\boldsymbol{B} = \{&\boldsymbol{r} \in \Re^3 | f_{\mathrm{db}}(\boldsymbol{r}) \le \gamma \quad \text{and} \\ &-[V(\boldsymbol{r}) + \boldsymbol{T}_{\mathrm{OL}}^T \boldsymbol{r}] \le (C_0 + \Delta J_{\max}) \quad \text{and} \\ &\exists \text{ a path from } \boldsymbol{r} \text{ to } \boldsymbol{r}_0\}\end{aligned}$$

We can define $r_{\max}$ and $v_{\max}$ similarly to the local case [Eqs. (24) and (25)] by substituting the set $\boldsymbol{B}$ for $\boldsymbol{A}$. Computation of $r_{\max}$ and $v_{\max}$ in the global case involves solving simultaneous implicit equations and is generally more complicated than obtaining the localized result. If the dead band is of sufficient dimension and oriented properly such that these values are finite, then the function $\beta(a) = r_{\max} + v_{\max}$ satifies the condition for boundedness.

B. Maximum Allowable Perturbations in Initial State

We can formulate the largest perturbations in initial state that a spacecraft subject to hovering control designed for a particular position can withstand and have the future motion remain bounded. Unlike the linearized result, there are two limits for ΔJ: a maximal decrease that can only be achieved by errors in position, and a maximal increase, achievable by a combination of errors in position and velocity. The following formulation applies only to hovering trajectories that are nominally bounded.

Without approximation, we define the zero-velocity surface as

$$\boldsymbol{Z} = \{\boldsymbol{r} \in \Re^3 | G(\boldsymbol{r}) = J(\boldsymbol{r}, \boldsymbol{0}) - C^* = 0\} \tag{26}$$

The bounding surface(s) created by the dead-band control can be defined by

$$\boldsymbol{D} = \{\boldsymbol{r} \in \Re^3 | d(\boldsymbol{r}) = f_{\mathrm{db}}(\boldsymbol{r}) - \gamma = 0\} \tag{27}$$

For boundedness to be preserved, C^* must be such that these surfaces fully enclose the permitted motion from the nominal hovering position. The critical values of C^* where hovering becomes unbounded occur when the zero-velocity surface and the control surfaces no longer intersect transversely, i.e., when there first exists a position $\boldsymbol{r} \in (\boldsymbol{Z} \cap \boldsymbol{D})$ such that $\nabla G(\boldsymbol{r})$ and $\nabla d(\boldsymbol{r})$ are colinear. Finding this critical point under the assumption that $\Delta J > 0$ yields the maximal allowable increase in Jacobi constant and assuming $\Delta J < 0$ gives the maximal decrease in Jacobi constant, ΔJ_+ and ΔJ_- can be found analytically in simplified cases and numerically in general.

This concept may be best demonstrated visually. Figures 4a and 4b show a series of zero-velocity surfaces, $\boldsymbol{Z}$, for different values of the Jacobi constant in the planar, circular-restricted three-body problem as dashed contour lines. Here, we assume that we are "hovering" at the $L1$ Lagrange point ($X \approx -609$ km, $Y = 0$ km) which requires no thrust because it is a natural equilibrium of the system. The control surfaces for a one-dimensional dead band, $\boldsymbol{D}$, are shown as vertical dotted lines. In this plot, a spacecraft's motion is restricted to areas where $J(\boldsymbol{r}, \boldsymbol{0})$ [equivalent to the negative of the potential $V(\boldsymbol{r})$ because there is no open-loop thrust] is less than the initial Jacobi constant. Beginning with the nominal energy at the hovering point (≈ -1.57), we can see that if we increase the energy to -1.35 (by increasing the initial velocity), the allowable region of motion created by the zero-velocity surface and the control surfaces expands but the allowable trajectory remains enclosed. It can be seen in the figure that at -1.28, ΔJ_+ has been exceeded. The zero-velocity contour and the control surface no longer intersect transversely. This means that the trajectory of a spacecraft that starts at the $L1$ Lagrange point with an energy of -1.28 is not guaranteed to be bounded. An example of an unbounded trajectory with a Jacobi constant of -1.28 is shown as a solid line in the figures. Figure 4b shows a zoomed-in view of the trajectory escaping out of the open bottleneck between the zero-velocity and control surfaces.

Now, we give an example analytical calculation of ΔJ_+ and ΔJ_- for spacecraft motion under a one-sided, one-dimensional dead-band control (without the open-loop thrust component) near a spherical body. Here, we can assume that the nominal position is of the form $\boldsymbol{r}_0 = [x_0, 0, z_0]$ without loss of generality. The zero-velocity surface and dead-band control surfaces are defined as

$$\boldsymbol{Z} = \left\{\boldsymbol{r} \in \Re^3 | G(\boldsymbol{r}) = -\frac{1}{2}\omega^2(x^2 + y^2) - \frac{\mu_{\mathrm{CB}}}{|\boldsymbol{r}|} - C^* = 0\right\} \tag{28}$$

$$\boldsymbol{D} = \{\boldsymbol{r} \in \Re^3 | d(\boldsymbol{r}) = x - R_c = 0\} \tag{29}$$

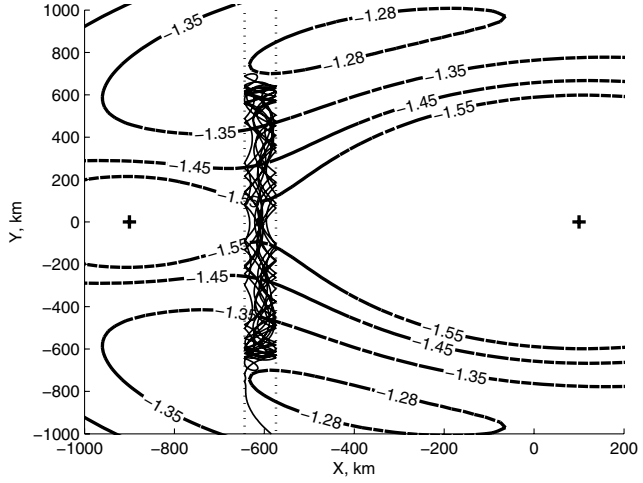

a)

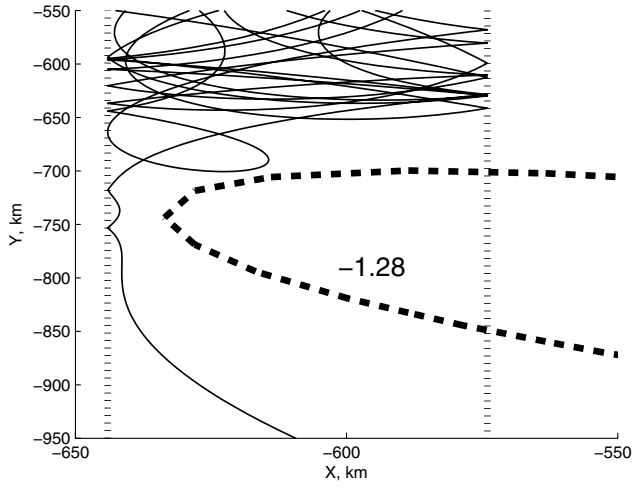

b)

Fig. 4 Escape trajectory in the restricted three-body problem; contours are zero-velocity surfaces for different initial energies, vertical dotted lines are the control boundaries.

For a trajectory in this system to be nominally bounded under one-dimensional control, $R_c < |\boldsymbol{r}_0| < R_r$ where

$$R_r = \left(\frac{\mu_{\mathrm{CB}}}{\omega^2}\right)^{1/3} \tag{30}$$

is the resonance radius. The applicable gradients are

$$\nabla G(\boldsymbol{r}) = \left[-\omega^2 x + \mu_{\mathrm{CB}}\frac{x}{|\boldsymbol{r}|^3}, -\omega^2 y + \mu_{\mathrm{CB}}\frac{y}{|\boldsymbol{r}|^3}, \mu_{\mathrm{CB}}\frac{z}{|\boldsymbol{r}|^3}\right], \quad \nabla d(\boldsymbol{r}) = [1,0,0] \tag{31}$$

We are seeking the Jacobi constant at the critical position $\boldsymbol{r}^* \in (\boldsymbol{Z} \cap \boldsymbol{D})$ where $\nabla G(\boldsymbol{r}^*)$ and $\nabla d(\boldsymbol{r}^*)$ are colinear. We can immediately see that $z^* = 0$ and $x^* = R_c$. There are three possible solutions for the y^* coordinate, $y^* = 0, \pm\sqrt{R_r^2 - R_c^2}$. The solution $[x^*, y^*, z^*] = [R_c, 0, 0]$ defines the largest allowable decrease in the Jacobi constant, $\Delta J_- = J([R_c, 0, 0], \mathbf{0}) - C_0$. This bound can only be violated by an error initial position such that the spacecraft is initially outside the dead band. The largest allowable increase in initial Jacobi constant is defined by the other two solutions for y^* where $\Delta J_+ = J([R_c, \pm\sqrt{R_r^2 - R_c^2}, 0], \mathbf{0}) - C_0$. If we consider only errors in initial velocity, we find

$$\delta v_{0,\max} = \sqrt{2\Delta J_+} \tag{32}$$

is the maximal allowable error in initial velocity such that the trajectory remains bounded. For hovering positions outside of the resonance radius, these solutions are not applicable because the hovering trajectory is not nominally bounded by this dead-band control.

VII. Particular Cases Applicable to Small Bodies

We can discuss a number of time-invariant systems that occur in spacecraft dynamics with equations of motion of the form in Eq. (1). In this section, we discuss boundedness of hovering in three systems commonly used to model dynamics near small bodies: the two-body problem in a rotating frame, the restricted three-body problem, and the Hill problem. Because J is well defined and twice differentiable at all physically relevant positions in these problems, the necessary type of dead-band control to bound hovering can be mapped as a function of hovering position. Unbounded or problematic hovering areas (near a boundary of the eigenvalue regions) for a particular controller can easily be identified and avoided.

A. Hovering in the Body-Fixed Frame (Two-Body Problem)

First, we determine the control type necessary to bound hovering in a coordinate frame rotating with a small body. It may be desirable to hover in the body-fixed frame for purposes of taking high-resolution measurements of a particular area of the surface or during a landing or sampling maneuver.

For this problem, we assume that hovering is performed close enough to the small body to consider it a two-body problem. We assume that the small body rotates uniformly about its maximum moment of inertia, which we align with the z-axis. We allow the small body to have an arbitrary shape, but assume its density to be uniform so that the gravitional potential is defined in closed form [8]. In this formulation, no solar effects are included. We assume that the spacecraft mass is negligible compared to that of the small body. The only forces present are the gravity of the small body, inertial forces due to the rotating frame, and the spacecraft thruster forces. The equations of motion for a spacecraft under body-fixed hovering control near a small body are

$$\ddot{x} - 2\omega\dot{y} = \omega^2 x + \frac{\partial U}{\partial x} + T_{\mathrm{OL},x} + T_{\mathrm{DB},x} \tag{33}$$

$$\ddot{y} + 2\omega\dot{x} = \omega^2 y + \frac{\partial U}{\partial y} + T_{\mathrm{OL},y} + T_{\mathrm{DB},y} \tag{34}$$

$$\ddot{z} = \frac{\partial U}{\partial z} + T_{\mathrm{OL},z} + T_{\mathrm{DB},z} \tag{35}$$

Here, the second subscript of the thrusts indicate the component of the vector to be used. Equations (33–35) define a conservative Lagrangian system in the form of Eq. (1) with Jacobi constant J_{bf}.

$$J_{\mathrm{bf}} = \frac{1}{2}|\boldsymbol{v}|^2 - \frac{1}{2}\omega^2(x^2 + y^2) - U(\boldsymbol{r}) - \boldsymbol{T}_{\mathrm{OL}}^T\boldsymbol{r} \tag{36}$$

The Hessian partial matrix with respect to position of J_{bf} is

$$\left.\frac{\partial^2 J_{\mathrm{bf}}}{\partial \boldsymbol{r}^2}\right|_{(\boldsymbol{r}_0,\mathbf{0})} = \begin{bmatrix} -\omega^2, & 0, & 0 \\ 0, & -\omega^2, & 0 \\ 0, & 0, & 0 \end{bmatrix} - \left.\frac{\partial^2 U}{\partial \boldsymbol{r}^2}\right|_{\boldsymbol{r}_0} \tag{37}$$

The signs of the eigenvalues of this matrix, and hence, the type of controller necessary for bounded hovering in the body-fixed two-body problem, can be mapped out for any well-defined potential field. Figure 5 shows the different eigenvalue regions for hovering positions above a spherical body in the X–Z plane, normalized by the resonance radius. The equations of motion are rotationally symmetric about the z-axis, so this figure fully characterizes the three-dimensional space around the body. Using the Routh criterion, it can be shown analytically that the boundary between the $+, +, -$ and the $+, -, -$ regions is precisely defined by a sphere at the center

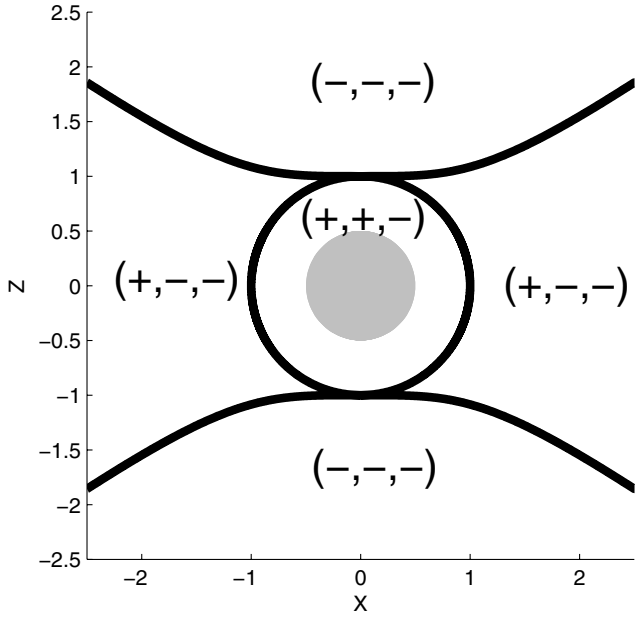

Fig. 5 Hovering regions near a spherical small body (normalized by the resonance radius).

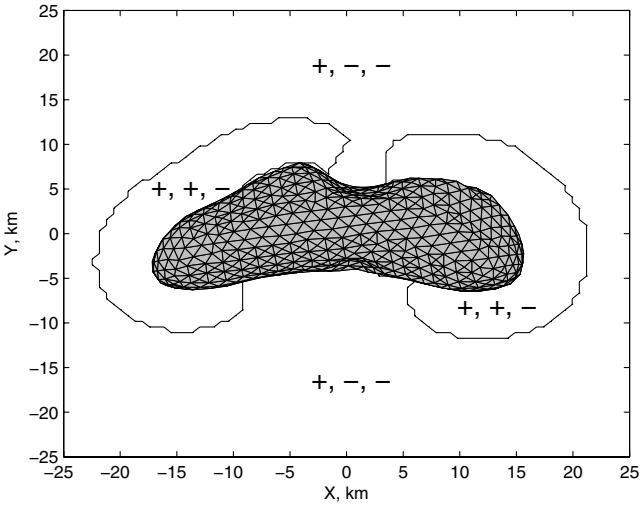

Fig. 6 Hovering regions near asteroid 433 Eros, *X–Y* plane.

of mass with radius equal to the resonance radius [Eq. (30)]. That is, all hovering positions near a spherical body with $|\boldsymbol{r}| < R_r$ have the +, +, − eigenvalue structure and therefore, can be bounded by a hovering controller with a one-dimensional dead band. Similarly, the boundary between the −, −, − and +, −, − regions is defined as a function of $|\boldsymbol{r}|$ for $|\boldsymbol{r}| > R_r$ by Eqs. (38) and (39).

$$\left(\frac{x}{R_r}\right)^2 = \frac{2}{3}\left(\frac{|\boldsymbol{r}|}{R_r}\right)^2 - \frac{2}{3}\left(\frac{R_r}{|\boldsymbol{r}|}\right) \tag{38}$$

$$\left(\frac{z}{R_r}\right)^2 = \frac{1}{3}\left(\frac{|\boldsymbol{r}|}{R_r}\right)^2 + \frac{2}{3}\left(\frac{R_r}{|\boldsymbol{r}|}\right) \tag{39}$$

Because no +, +, + regions exist in this problem, we have analytically defined the shape of the zero-velocity surface for hovering near a sphere as a function of position. Nothing in this analysis limits the results to small bodies; the eigenvalue regions defined in Fig. 5 apply equally well to dynamics near spherical planetary bodies. However, on the planetary scale, the necessary thrust to hover is large and the oscillations from nominal allowed under a bounding controller may be too large for some applications.

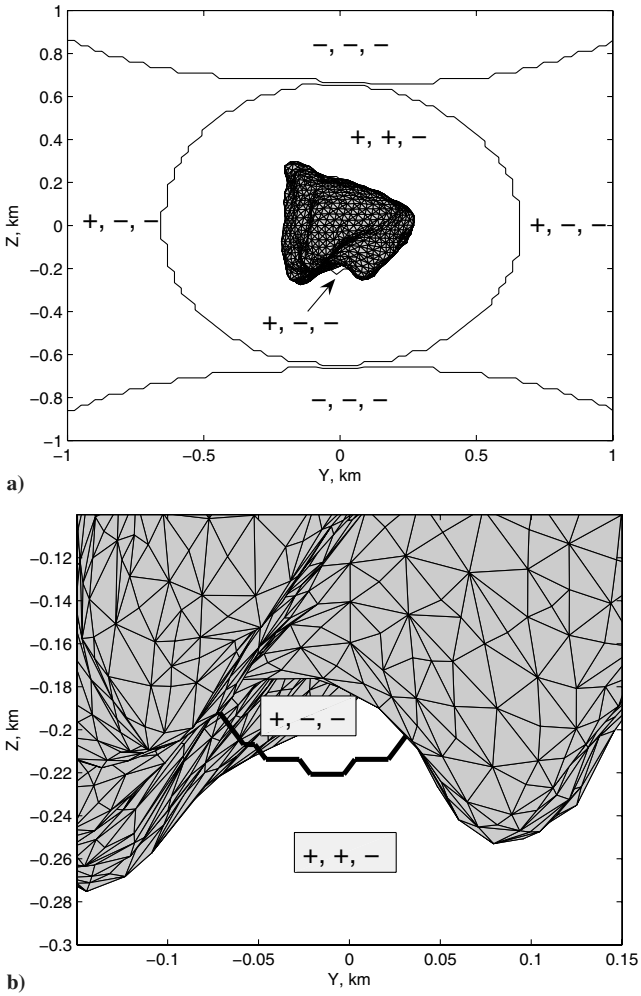

Fig. 7 Hovering regions near asteroid 6489 Golevka, *Y–Z* plane.

The eigenvalue regions are more complex to define for real small body shapes. Because the term "small body" covers a wide range of irregular gravitational fields, the shape of the eigenvalue regions is unique to each. Figure 6 shows the sufficient dead band for bounded hovering in the equatorial plane near a polyhedral model of the asteroid 433 Eros (3.0 g/cm^3 density, 5.27 h period) [9]. Because of Eros' elongated shape, the +, +, − hovering region here is divided into two lobes. Hovering above the small body equator requires a one-dimensional dead band near the elongated ends of the body and requires two dimensions of dead-band control near its midsection. Figure 7 shows the different hovering regions near a polyhedral model of the asteroid 6489 Golevka (5.0 g/cm^3 density, 6.0289 h period) [10]. This is also interesting because of the +, −, − region inside the large canyon that runs across Golevka's south pole.

B. Hovering in the Restricted Three-Body Problem

Next we look at hovering in the restricted three-body problem. It may be advantageous to hover in this frame which rotates with the small body around the sun for the purpose of keeping a fixed communication, sensing, or solar panel geometry. This formulation can be applied to hovering in the small-body–sun system, a planet–moon system, or a binary asteroid system.

Here, we assume that both primaries have point-mass potential fields so that the equations of motion are time-invariant. More complex gravity fields can be used if the rotation rate of the bodies is equal to their mean motion around each other. Our equations are centered at the center of mass of the two primaries with the positive x-axis pointing towards the smaller primary. The z-axis is normal to the plane of the primaries' mutually circular orbit and completes the right-handed coordinate frame. The equations of motion for this system with hovering control are

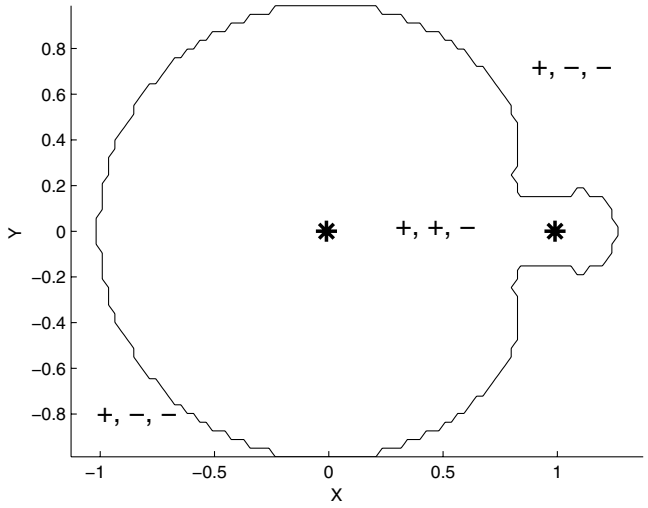

Fig. 8 Hovering regions in the restricted three-body problem; $\mu = 0.01$, X–Y plane (normalized by R, asterisks denote position of primaries).

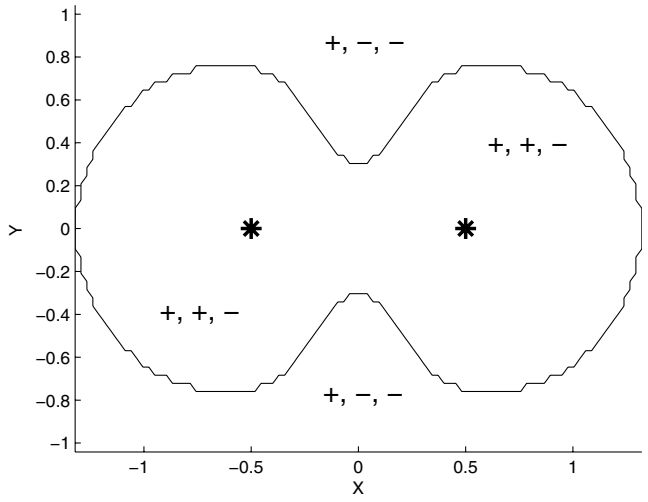

Fig. 9 Hovering regions in the restricted three-body problem; $\mu = 0.5$, X–Y plane (normalized by R, asterisks denote position of primaries).

$$\ddot{x} - 2N\dot{y} = N^2 x - \mu_1 \frac{x + \mu R}{|\boldsymbol{r}_{\mathrm{sc},1}|^3} - \mu_2 \frac{x - (1-\mu)R}{|\boldsymbol{r}_{\mathrm{sc},2}|^3} + T_{\mathrm{OL},x} + T_{\mathrm{DB},x} \tag{40}$$

$$\ddot{y} + 2N\dot{x} = N^2 y - \mu_1 \frac{y}{|\boldsymbol{r}_{\mathrm{sc},1}|^3} - \mu_2 \frac{y}{|\boldsymbol{r}_{\mathrm{sc},2}|^3} + T_{\mathrm{OL},y} + T_{\mathrm{DB},y} \tag{41}$$

$$\ddot{z} = -\mu_1 \frac{z}{|\boldsymbol{r}_{\mathrm{sc},1}|^3} - \mu_2 \frac{z}{|\boldsymbol{r}_{\mathrm{sc},2}|^3} + T_{\mathrm{OL},z} + T_{\mathrm{DB},z} \tag{42}$$

where $\boldsymbol{r}_{\mathrm{sc},1} = [x + \mu R, y, z]^T$, $\boldsymbol{r}_{\mathrm{sc},2} = [x - (1-\mu)R, y, z]^T$, and $N = \sqrt{(\mu_1 + \mu_2)/R^3}$. Again, this is a conservative Lagrangian system in the proper form with time-invariant Jacobi constant:

$$J_{\mathrm{R3BP}} = \frac{1}{2}|\boldsymbol{v}|^2 - \frac{1}{2}N^2(x^2 + y^2) - \frac{\mu_1}{|\boldsymbol{r}_{\mathrm{sc},1}|} - \frac{\mu_2}{|\boldsymbol{r}_{\mathrm{sc},2}|} - \boldsymbol{T}_{\mathrm{OL}}^T \boldsymbol{r} \tag{43}$$

Using the methodology discussed previously, we can map the dead-band control sufficient to bound hovering in the restricted three-body problem as a function of position. Figure 8 shows the shape of the eigenvalue regions in the vicinity of the two primaries for $\mu = 0.01$, a value typical for a planet–moon system. We can see that each primary has an area in its immediate vicinity proportional to its mass where hovering requires one-dimensional perturbation control. If we consider $\mu = 0.5$, representative a binary asteroid system, we find a $+, +, -$ region in the X–Y plane as shown in Fig. 9. Here, we can see a lobe of $+, +, -$ dynamics around each primary with the region being slightly larger on the outside of the primaries' orbit than on the inside.

C. Hovering in the Hill Three-Body Problem

Finally, we look at hovering in the Hill three-body problem, which is a valid approximation of the restricted three-body problem for hovering points near the smaller primary when μ is small. The Hill approximation does not apply to binary asteroid systems. The effects of solar radiation pressure are easily included in this formulation [11]. In the sun–small-body system, the equations of motion centered at the small body are

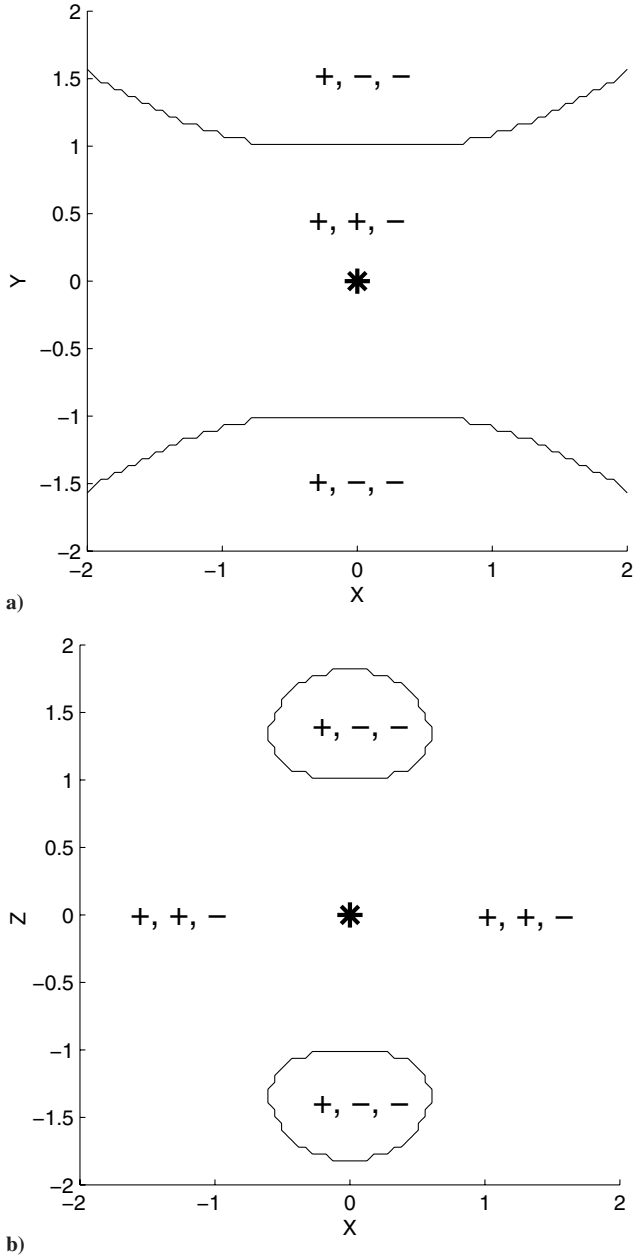

Fig. 10 Hovering regions in the Hill three-body problem; a) X–Y and b) X–Z planes (normalized by the Hill radius, asterisk denotes position of the primary).

$$\ddot{x} - 2N\dot{y} = 3N^2 x - \mu_{SB}\frac{x}{|\boldsymbol{r}|^3} + \frac{\beta_{SRP}}{R^2} + T_{OL,x} + T_{DB,x} \tag{44}$$

$$\ddot{y} + 2N\dot{x} = -\mu_{SB}\frac{y}{|\boldsymbol{r}|^3} + T_{OL,y} + T_{DB,y} \tag{45}$$

$$\ddot{z} = -N^2 z - \mu_{SB}\frac{z}{|\boldsymbol{r}|^3} + T_{OL,z} + T_{DB,z} \tag{46}$$

The time-invariant Jacobi constant is

$$J_{Hill} = \frac{1}{2}|\boldsymbol{v}|^2 - \frac{3}{2}N^2x^2 + \frac{1}{2}N^2z^2 - \frac{\mu_{SB}}{|\boldsymbol{r}|} + \frac{\beta_{SRP}x}{R^2} - \boldsymbol{T}_{OL}^T\boldsymbol{r} \tag{47}$$

The sufficient dead-band type to bound hovering near the small body is mapped the same way we have done previously. When $|\boldsymbol{r}| < r_{Hill}$ [Eq. (48)], the results are identical to those obtained in the full restricted three-body problem.

$$r_{Hill} = R\left(\frac{\mu_{SB}}{3(\mu_{SB} + \mu_{Sun})}\right)^{1/3} \tag{48}$$

Figure 10 shows the eigenvalue regions for hovering near the small body in the X–Z plane of the Hill problem. It can be noted that the addition of solar radiation pressure has no effect on the sufficient dead band because the potential associated with it is linear under Hill's approximations. The only difference in the necessary control is in $\boldsymbol{T}_{OL}$, which must null the nominal acceleration due to solar radiation pressure.

VIII. Discussion

A. Implementation of Bounded Hovering

Our main result is not that the spacecraft trajectory can be bounded by dead-band control, but that it can often be done by a reduced-order controller. For instance, hovering in close proximity to a small body (inside the resonance radius) as may be necessary for a sampling or landing maneuver can often be bounded by a one-dimensional dead-band controller, because the zero-velocity surface frequently has a $+$, $+$, $-$ structure. Further, the eigenvector corresponding to the negative eigenvalue (the direction the zero-velocity surface allows unrestricted motion) is usually closely aligned with the gravitational acceleration vector (unless hovering near the resonance radius), which means altimetry measurements may be considered as a basis for the dead-band control. At positions with $+$, $-$, $-$ zero-velocity surfaces, a dead-band control on the latitude and longitude of the spacecraft, possibly based on optical navigation measurements, may be a good candidate to bound the trajectory.

For safety purposes, it may be desirable to have three-dimensional control of the spacecraft motion as on the Hayabusa spacecraft [12]. This could be achieved by a three-dimensional dead-band controller, or more cleverly, by a combination of a one-dimensional [such as Eq. (10)] and a two-dimensional dead-band control [Eq. (11)]. Depending on where the spacecraft hovers, the γ parameter of each thrust control could be adjusted so that the minimal dimension controller bounds the spacecraft and the secondary controller, which has a larger γ value, provides a safety net. Measurements for the secondary dead band could be performed less frequently, which would conserve spacecraft resources.

B. Asymptotic Stability of Hovering

Ideally it is possible to achieve asymptotic stability of hovering by modifying the dead-band thrust control [Eq. (8)]. Hysteresis can be added to the dead band such that the reflected spacecraft speed becomes some fraction of the incoming speed. This causes the Jacobi constant to decrease in value after every dead-band thrust. In the $+$, $+$, $-$ case, the zero-velocity surface becomes a two-sheet hyperboloid and recesses away from the nominal hovering point as Jacobi constant decreases. The spacecraft motion is restricted to the space between one sheet of the hyperboloid and the dead-band control surface. In an idealized situation, this space eventually reduces to a single point, not at the nominal hovering position, but on the dead-band boundary. The other eigenvalue cases yield similar results. Hence, this controller would produce asymptotically stable hovering. Of course, asympotic stability in reality is not feasible with this controller due to thruster constraints. However, hysteresis may be useful to manipulate the Jacobi constant to decrease (or increase) the size of the bounded hovering region in accordance with mission goals.

IX. Conclusions

In this paper, we have developed sufficient conditions for a dead-band controller to bound spacecraft hovering motion in time-invariant Lagrangian dynamical systems. We found that if the dead-band control restricts motion in at least as many dimensions as the zero-velocity surface allows unrestricted motion (determined by the eigenvalues of the Hessian matrix of the Jacobi constant with respect to position) and it is aligned properly, then it is sufficient to bound perturbed trajectories near the induced equilibrium. This result can be used to identify hovering positions where it may be possible to use a dead-band control based on a reduced measurement set (i.e., one-dimensional control based on altimetry or two-dimensional control based on optical navigation measurements). We were able to map the sufficient dead-band dimensionality in the rotating two-body, restricted three-body, and Hill problems and found that hovering in close proximity to a small body usually only requires a one- or two-dimensional dead-band controller to stabilize motion.

Appendix: An Observation on Lagrangian Dynamics

The results we find for equilibria in spacecraft dynamical systems of the form of Eq. (1) are applicable to a broader class of unconstrained, time-invariant Lagrangian systems. This more general formulation follows.

For a time-invariant rheonomic system, there exists a Lagrangian function of the form

$$L(\boldsymbol{q}, \dot{\boldsymbol{q}}) = T(\boldsymbol{q}, \dot{\boldsymbol{q}}) + V(\boldsymbol{q}) \tag{A1}$$

The Jacobi constant is defined as

$$J(\boldsymbol{q}, \dot{\boldsymbol{q}}) = \frac{\partial L}{\partial \dot{\boldsymbol{q}}}\dot{\boldsymbol{q}} - L = C_L \tag{A2}$$

which has constant value for all states on a valid trajectory. The equations of motion for this system are given by the standard form of Lagrange's equation.

$$\dot{\boldsymbol{q}} = \dot{\boldsymbol{q}} \tag{A3}$$

$$\dot{\boldsymbol{p}} = \frac{\mathrm{d}}{\mathrm{d}t}\left(\frac{\partial L}{\partial \dot{\boldsymbol{q}}}\right) = \frac{\partial L}{\partial \boldsymbol{q}} \tag{A4}$$

For a state to be an equilibria, $\dot{\boldsymbol{q}}_{eqm} = 0$. In addition, $\partial L/\partial \boldsymbol{q}$ must equal zero. When evaluated at $\dot{\boldsymbol{q}}_{eqm}$, this second condition reduces to finding $\boldsymbol{q}_{eqm}$ such that $[\partial J(\boldsymbol{q}, \dot{\boldsymbol{q}})/\partial \boldsymbol{q}]|_{(\boldsymbol{q}_{eqm}, \boldsymbol{0})} = 0$.

The discussion follows from here in the same manner as in Sec. II. If the trajectory is initialized at the equilibrium point $(\boldsymbol{q}_{eqm}, \boldsymbol{0})$, all possible future states must have the same value of Jacobi constant. A quadratic expansion around the equilibrium can be performed and because $|\dot{\boldsymbol{q}}| > 0$, this defines the zero-velocity surface of the system in the vicinity of the equilibrium.

Acknowledgments

The research described in this paper was sponsored by the Interplanetary Network Technology Program by a grant to The University of Michigan from the Jet Propulsion Laboratory, California Institute of Technology which is under contract with NASA. S. B. Broschart was also supported by the NASA Graduate

Student Researchers Program and by the Michigan Space Grant Consortium. The authors graciously acknowledge the contribution of Jesse B. Hoagg during the revision process.

References

[1] Scheeres, D. J., "Stability of Hovering Orbits Around Small Bodies," *Spaceflight Mechanics 1999*, Advances in the Astronautical Sciences, Vol. 102, Pt. 2, Univelt, San Diego, CA, 1999, pp. 855–875.

[2] Sawai, S., Scheeres, D. J., and Broschart, S. B., "Control of Hovering Spacecraft Using Altimetry," *Journal of Guidance, Control, and Dynamics*, Vol. 25, No. 4, 2002, pp. 786–795.

[3] Broschart, S. B., and Scheeres, D. J., "Control of Hovering Spacecraft near Small-Bodies: Application to Asteroid 25143 Itokawa," *Journal of Guidance, Control, and Dynamics*, Vol. 28, No. 2, 2005, pp. 343–354.

[4] Kubota, T., Hashimoto, T., Uo, M., Maruya, M., and Baba, K., "Maneuver Strategy for Station Keeping and Global Mapping Around an Asteroid," *Spaceflight Mechanics 2001*, Advances in the Astronautical Sciences, Vol. 108, Univelt, San Diego, CA, 2001, pp. 769–779.

[5] Kominato, T., Matsuoka, M., Uo, M., Hashimoto, T., and Kawaguchi, J., "Optical Hybrid Navigation in Hayabusa Approach, Station Keeping, & Hovering," AAS Paper 06-209, Jan. 2006.

[6] Selby, S. M., *CRC Standard Mathematical Tables*, 21st ed., Chemical Rubber Company, Cleveland, OH, 1973.

[7] Khalil, H. K., *Nonlinear Systems*, 3rd ed., Prentice–Hall, Upper Saddle River, NJ, 2002.

[8] Werner, R. A., and Scheeres, D. J., "Exterior Gravitation of a Polyhedron Derived and Compared with Harmonic and Mascon Gravitation Representations of Asteroid 4769 Castalia," *Celestial Mechanics and Dynamical Astronomy*, Vol. 65, No. 3, 1996, pp. 313–344.

[9] Scheeres, D. J., Williams, B. G., and Miller, J. K., "Evaluation of the Dynamic Environment of an Asteroid: Applications to 433 Eros," *Journal of Guidance, Control, and Dynamics*, Vol. 23, No. 3, 2000, pp. 466–475.

[10] Hudson, R. S., Ostro, S. J., Jurgens, R. F., Rosema, K. D., Giorgini, J. D., Winkler, R., Rose, R., Choate, D., Cormier, R. A., Franck, C. R., Frye, R., Howard, D., Kelley, D., Littlefair, R., Slade, M. A., Benner, L. A. M., Thomas, M. L., Mitchell, D. L., Chodas, P. W., Yeomans, D. K., Scheeres, D. J., Palmer, P., Zaitsev, A., Koyama, Y., Nakamura, A., Harris, A. W., and Meshkov, M. N., "Radar Observations and Physical Modeling of Asteroid 6489 Golevka," *Icarus*, Vol. 148, No. 1, 2000, pp. 37–51.

[11] Scheeres, D. J., and Marzari, F., "Spacecraft Dynamics in the Vicinity of a Comet," *Journal of the Astronautical Sciences*, Vol. 50, No. 1, 2002, pp. 35–52.

[12] Kubota, T., Hashimoto, T., Sawai, S., Kawaguchi, J., Ninomiya, K., Uo, M., and Baba, K. , "An Autonomous Navigation and Guidance System for MUSES-C Asteroid Landing," *Acta Astronautica*, Vol. 52, Nos. 2–6, 2003, pp. 125–131.